


RESEARCH ARTICLE

Open Access



Calcium currents in striatal fast-spiking interneurons: dopaminergic modulation of Ca_v1 channels

Ernesto Alberto Rendón-Ochoa, Teresa Hernández-Flores, Víctor Hugo Avilés-Rosas, Verónica Alejandra Cáceres-Chávez, Mariana Duhne, Antonio Laville, Dagoberto Tapia, Elvira Galarraga and José Bargas* 

Abstract

Background: Striatal fast-spiking interneurons (FSI) are a subset of GABAergic cells that express calcium-binding protein parvalbumin (PV). They provide feed-forward inhibition to striatal projection neurons (SPNs), receive cortical, thalamic and dopaminergic inputs and are coupled together by electrical and chemical synapses, being important components of the striatal circuitry. It is known that dopamine (DA) depolarizes FSI via D_1 -class DA receptors, but no studies about the ionic mechanism of this action have been reported. Here we ask about the ion channels that are the effectors of DA actions. This work studies their Ca^{2+} currents.

Results: Whole-cell recordings in acutely dissociated and identified FSI from PV-Cre transgenic mice were used to show that FSI express an array of voltage gated Ca^{2+} channel classes: Ca_v1 , $Ca_v2.1$, $Ca_v2.2$, $Ca_v2.3$ and Ca_v3 . However, Ca_v1 Ca^{2+} channel carries most of the whole-cell Ca^{2+} current in FSI. Activation of D_1 -like class of DA receptors by the D_1 -receptor selective agonist SKF-81297 (SKF) enhances whole-cell Ca^{2+} currents through Ca_v1 channels modulation. A previous block of Ca_v1 channels with nifedipine occludes the action of the DA-agonist, suggesting that no other Ca^{2+} channel is modulated by D_1 -receptor activation. Bath application of SKF in brain slices increases the firing rate and activity of FSI as measured with both whole-cell and Ca^{2+} imaging recordings. These actions are reduced by nifedipine.

Conclusions: The present work discloses one final effector of DA modulation in FSI. We conclude that the facilitatory action of DA in FSI is in part due to Ca_v1 Ca^{2+} channels positive modulation.

Keywords: Ca^{2+} -currents, Ca^{2+} -channels, Fast-spiking interneurons, Dopamine, D_1 -like dopamine receptors, Excitability

Background

Inhibitory GABAergic interneurons are part of striatal circuitry. They control striatal projection neurons output (SPNs), are a part of neuronal ensembles and participate in cognition, procedural learning and motor performance [1–8]. Among all striatal interneurons, parvalbumin-positive (PV+) fast spiking interneurons

(FSI) are the most studied. They can fire at high frequencies with little adaptation and represent about 0.7% of the total neuronal population. Although the proportion of PV+ interneurons is small compared to spiny projection neurons (SPN), they have physiological relevance by providing feed forward perisomatic and dendritic inhibition to large numbers of SPNs [1, 2, 9]. FSI receive inputs from cortical and thalamic regions [3, 10, 11], are interconnected by gap junctions and GABAergic chemical synapses that may help to generate synchronized or correlated firing between them. Activation of FSI has widespread effects upon SPNs [12, 13].

*Correspondence: jbargas@ifc.unam.mx
División de Neurociencias, Instituto de Fisiología Celular, Universidad Nacional Autónoma de México, Circuito Exterior s/n Ciudad Universitaria, Col. Coyoacán, 04510 Ciudad de México, México



Striatal neurons receive massive dopaminergic innervation from the substantia nigra pars compacta (SNc) [14–16]. In vitro studies have shown that dopamine is an important modulator in the striatum which shapes excitability and circuitry management through, in part, the control of different receptors, ion channels, such as K^+ , Ca^{2+} and synaptic channels, neurons and neuronal ensembles [17–19]. In FSI, DA binds to D5-type dopamine receptors, a member of the D1-class receptors [20, 21]. Activation of these receptors produces a depolarization accompanied by action-potential (AP) discharge in striatal FSI [20, 21], as well as in FSI from the prefrontal cortex [22, 23] and basolateral amygdala [24]. Although DA receptors expressed in striatal FSI are known, no description about their functional effectors has been made. In SPNs, dopamine modulates Ca^{2+} entry through somatic Ca_v1 , $Ca_v2.1$ and $Ca_v2.2$ currents [25, 26] regulating firing frequency [25, 27]. In striatal cholinergic interneurons (CHI), dopamine modulates whole-cell Ca^{2+} current regulating firing properties, as well as the time course and shape of action potentials (AP) [28]. However, no study has been made to know whether calcium channels are involved on the depolarization produced by dopamine in FSI. Hence, this study was proposed to find out: (1) the Ca^{2+} channel classes expressed in FSI, (2) if there is dopaminergic modulation of Ca^{2+} currents in FSI, and finally, (3) whether there are particular Ca^{2+} channels modulated by dopamine receptors. Accordingly, as a first approach, we use whole-cell recording in acutely dissociated striatal and identified FSI obtained from transgenic PV-cre mice in order to avoid indirect actions. Besides, whole cell current clamp recordings in slices as well as dynamic Ca^{2+} imaging with single cell resolution were performed. All techniques confirmed the hypothesis that D1-class receptor agonists enhance Ca^{2+} current carried by Ca_v1 channel leading to an increase in excitability of striatal FSI.

Methods

Experimental subjects and design

Experimental subjects, obtained from IFC bioterium were: B6; 12P2-*Pvalb*^{tm1(cre)Arbr}/J (PV-Cre; Silvia Arber, Friederich Miescher Institute; Jackson Labs, stock# 008069), called PV+ mice from now on. Experimental subjects were housed in acrylic cages (4–5 mice per cage; 19 × 29 × 12 cm) with wood-based bedding and cardboard cylinders, kept on a 12:12 light/dark (light beginning at 8 am) period with a temperature maintained at 20–21 °C in IFC vivarium after surgery (see below) until used for experiments. All animals had standard rodent chow and water ad libitum. In order to identify isolated PV+ interneurons, PV-Cre transgenic mice at PD 21 (21 days, mean ± 4 days, 30 g mean ± 4, at 14–18 h),

were anesthetized i.p. with ketamine (Bayer 75 mg/kg) and xilazine (Bayer 10 mg/kg) and injected stereotaxically in a laminar flow hood (Telsar technologies. Model PV-30/60) in a dedicated, sterile room, with the following viral constructs (University of Pennsylvania Vector Core): AAV2/1.CAG.Flex.tdTomato.WPRE.bGH (Hongkui Zeng) for whole cell recordings in isolated cells, AAV1.Syn.Flex.GCaMP6f.WPRE.SV40 [29], for calcium imaging recordings and AAV1.CAG.Flex.eGFP.WPRE.bGH (Allen institute) for some current clamp experiments in slices at the following coordinates relative to bregma (in mm): AP=0.9, ML=±1.2, DV=-3.2. The total virus volume injected was 0.8 µl over a period of 10 min (Fig. 1a). Animals were monitored for two weeks to ensure full recovery and fluorescent protein expression (Fig. 1b). A total of 45 infected PV-Cre mice were randomly assigned to 6 independent groups: for voltage clamp recordings of calcium currents (see next sections for details of the techniques) to observe contribution of Ca^{2+} channels classes (Fig. 2; n=19 recordings from 18 different mice, below); effects of DA on Ca^{2+} currents (Fig. 3a, b; n=8 recording from 8 different mice); SCH+SKF control group (Fig. 3c, d; n=6 recordings from 4 different mice); nicardipine on DAergic actions (Fig. 4; n=8 recordings from 6 different mice); current clamp recordings in slices (Fig. 5; n=6 recordings from 6 different mice for SKF-nicardipine experiments and n=4 for SKF-SCH experiments) and calcium imaging experiments (Fig. 6; n=33; for imaging PV-cre identified FSI were extracted from 6 different experiments/slices from 3 different mice). The experimental units were single neuron recordings or changes in fluorescence ($\Delta F/F$ where ΔF =changes in fluorescence and F =basal fluorescence). Subject numbers were minimized to obtain statistical significance.

Preparation of dissociated neurons and slices

Brain slices and acutely dissociated neurons were obtained and described in previous work [30–34]. Briefly, infected PV-Cre mice were anesthetized (see above). The mice were decapitated, their brains were removed and submerged in iced saline solution containing (in mM): 126 NaCl, 3 KCl, 26 NaHCO₃, 2 CaCl₂, 1 MgCl₂, 11 glucose, 0.2 thiourea and 0.2 of ascorbic acid (25 °C; pH: 7.4 with HCl, 300 ± 5 mOsm/l with glucose; saturated with 95% O₂ and 5% CO₂). Using a vibratome (1000 Classic, Warner Instruments, Hamden, USA), sagittal brain slices of 300 µm thick were cut and placed in the same saline solution for 1 h at 34 °C. When recordings were done in slices, they were transferred to a submerged chamber and superfused at 5 ml/min with saline solution. When recordings were done in dissociated cells, the dorsal striatum was dissected from the slices and returned into the

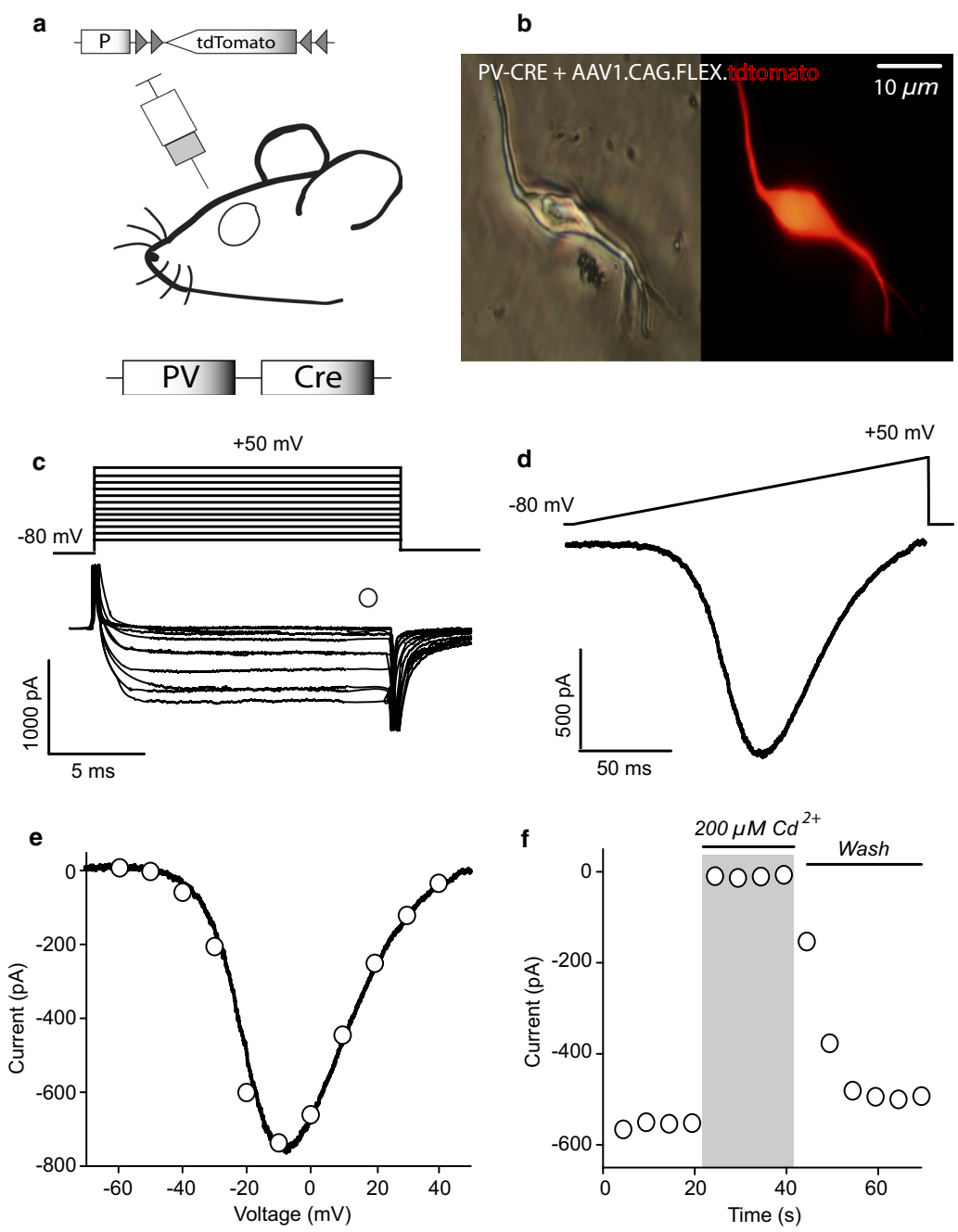
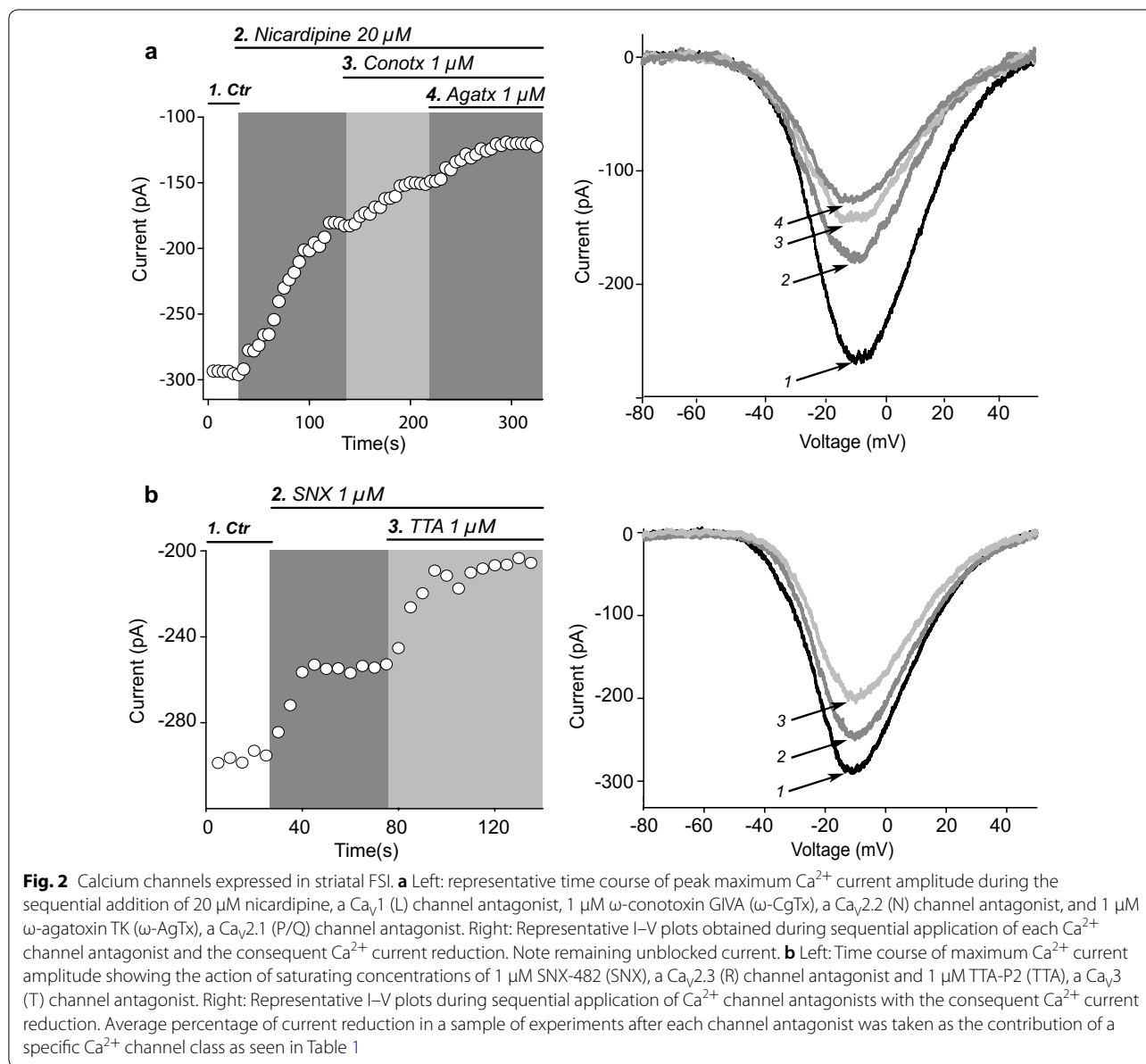


Fig. 1 Whole-cell Ca^{2+} currents in acutely dissociated FSI. **a** Schematic infection protocol in PV-cre mice with a viral construction containing tdTomato into the dorsal striatum. **b** Representative images of virally infected, acutely dissociated PV-cre FSI. Left: light microscopy; right: the same fluorescent tdTomato PV-cre cell. **c** Inward currents (bottom) elicited by rectangular voltage commands from -80 to $+50$ mV (top) in 10 mV steps (tail currents are clipped). Empty circle shows where the amplitude current measurements were obtained. **d** Inward current in the same neuron elicited by a ramp command from -80 to $+50$ mV (0.7 mV/ms). **e** Current–voltage relationship (I–V plot). Empty circles are measurements taken from currents elicited with voltage commands (as in **c**) and continuous line was the current obtained with the ramp command (as in **d**). Measurements using both protocols are superimposed. Note that measurements using the ramp command appear to “fit” measurements using the square commands suggesting good voltage control and space clamp. **f** Representative time course of Ca^{2+} current blockade during bath application of $200 \mu\text{M Cd}^{2+}$



saline solution containing 10 mM HEPES plus 0.5 mg/ml of papain (*Carica papaya*; Calbiochem, Cat# 5125. San Diego CA) at 34 °C. After 20–25 min of digestion, the striatum slices were transferred to a low Ca^{2+} (0.4 mM CaCl_2) saline solution. To obtain individual cells, the striatal slices were mechanical dissociated with a graded series of fire-polished Pasteur pipettes. The cell suspension (1 ml) was plated into a Petri dish mounted on the stage of an inverted microscope (Nikon Instruments, Melville, NY, 20 ×/0.4 NA). Cells were left for 10–15 min for neurons to adhere to the bottom of the dish. The dish contained 1 ml of the whole-cell recording saline solution (in mM): 0.001 tetrodotoxin (TTX), 140 NaCl, 3 KCl, 5

BaCl_2 , 2 MgCl_2 , 10 HEPES, and 10 glucose (pH: 7.4 with NaOH; 300 ± 5 -mOsm/l with glucose). Thereafter, the cells were superfused at 1 ml/min with saline of the same composition at room temperature (approximate 25 °C). Tomato-positive neurons were visualized using a UV lamp (X-Cite; EXFO, Ontario, Canada; Fig. 1b). Dissociated neurons lack their distal dendrites and axon, so currents reported are somatic.

Voltage clamp recordings of calcium currents

Voltage-clamp recordings were performed on identified striatal PV+ interneurons with 12–15 μm soma diameter and whole-cell capacitance of 6–7 pF with short or

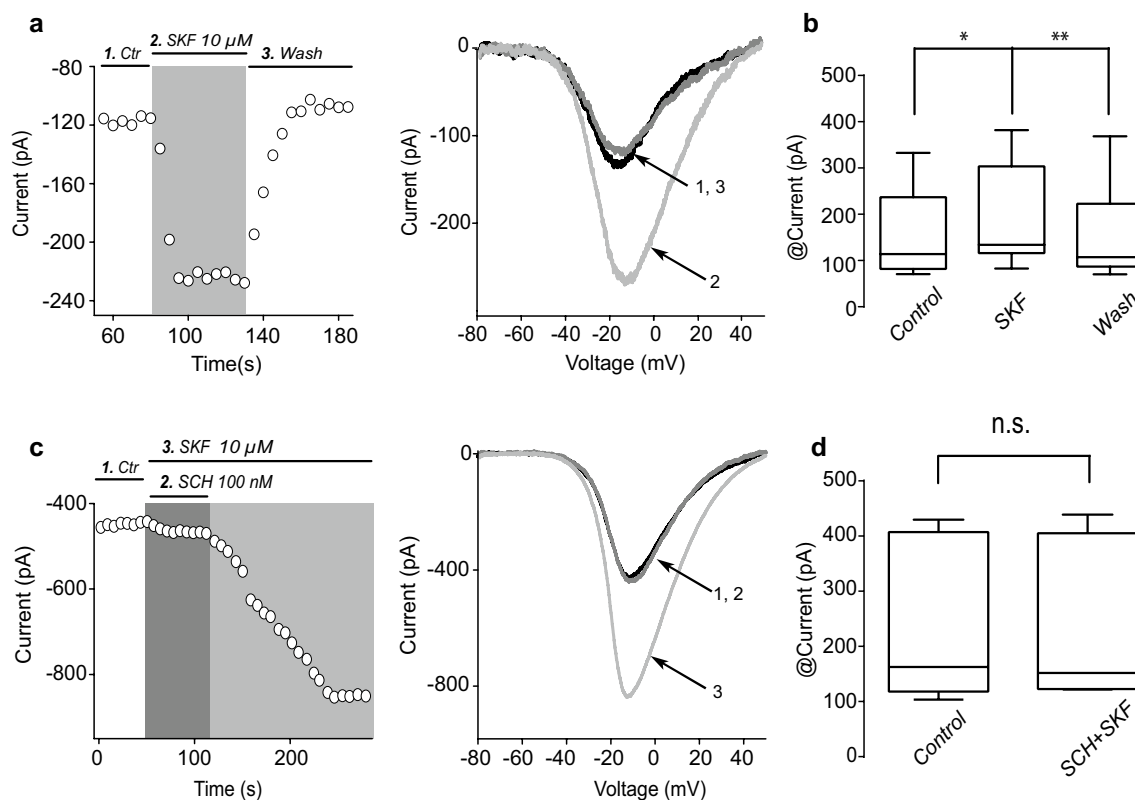


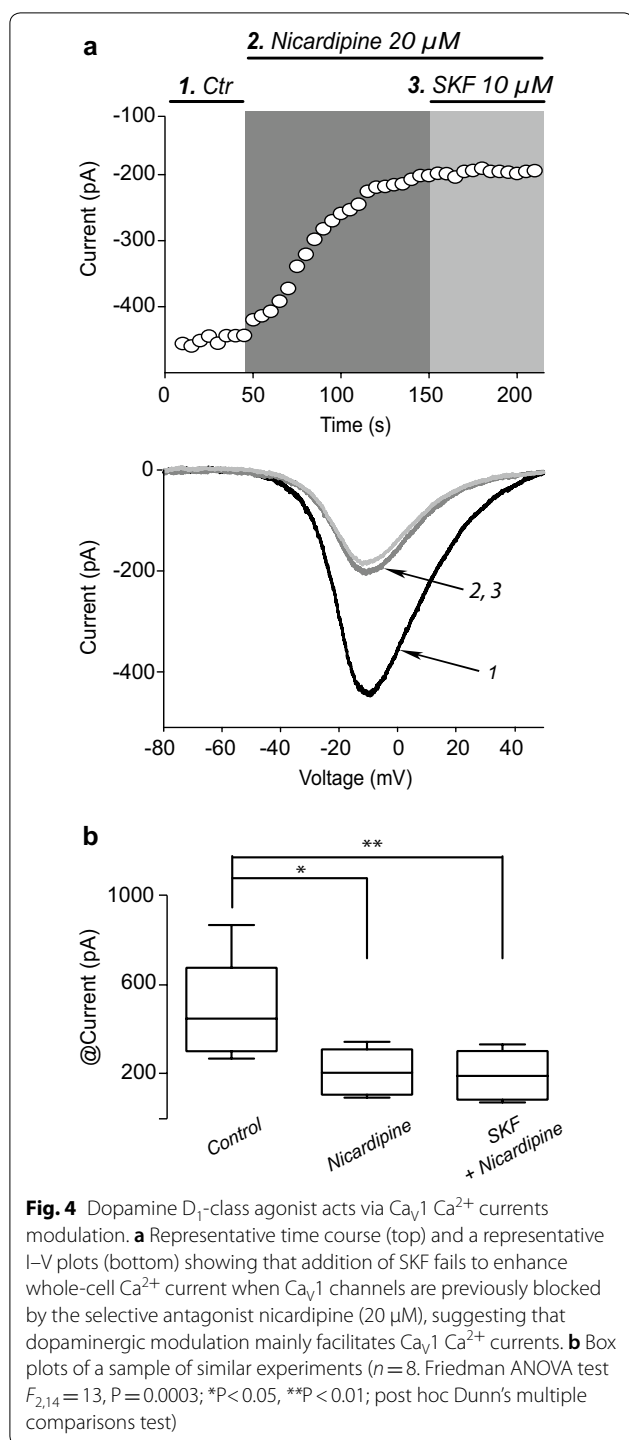
Fig. 3 Activation of D1-class DA receptors enhances whole-cell Ca^{2+} currents in FSL. **a** Left: Representative time course (left) and representative I-V plots (right) showing that activation of D1-like DA receptors by addition of the selective DA agonist 10 μM SKF-81297 (SKF) to the bath solution enhances control Ca^{2+} currents. **b** Box plots summary of absolute Ca^{2+} current amplitudes in control, during SKF and after washing the agonist ($n=8$; Friedman ANOVA test $F_{2,14}=13$, $P=0.0003$; $*P<0.05$, $**P<0.01$; post hoc Dunn's multiple comparisons test). **c** Time course of maximum Ca^{2+} current showing specific blockade of SKF actions by the selective DA receptor antagonist 100 nM SCH-23390 (SCH) in the presence of SKF. Removal of SCH leads to an enhancement of Ca^{2+} current by SKF. Representative I-V plots at right. **d** Box plot summarizing the absolute current amplitude in control conditions and during addition of SCH plus SKF ($n=8$; $P=0.99$; Wilcoxon T test)

absent dendritic trunks [32, 34]. Patch pipettes of borosilicate glass (WPI, Sarasota, FL, USA) were pulled in a Flaming-Brown puller (Sutter Instrument Corporation, Novato, CA, USA) and fire polished prior to use. The internal saline solution contained (in mM): 180 N-methyl-D glucamine (NMDG), 40 HEPES, 10 EGTA, 4 MgCl_2 , 2 ATP, 0.4 GTP and 0.1 leupeptin (pH=7.2 with H_2SO_4 ; 280 ± 5 mOsm/l; room temperature around 25 $^\circ\text{C}$). Whole-cell recordings used electrodes with D.C. resistance of 3–6 $\text{M}\Omega$ in the bath. Liquid junction potentials (5–10 mV) were corrected. Recordings of Ca^{2+} currents were obtained with an Axopatch 200B patch-clamp amplifier (Axon Instruments, Foster City, CA, USA) and controlled and monitored with pClamp (version 8.2, RRID: rid_000085) and a 125 kHz DMA interface (Axon Instruments, Foster City, CA, USA). We recorded currents passing through Ca^{2+} channels using Ba^{2+} as a charge carrier as shown in previous articles [31, 34, 35]. Ba^{2+} is a potent K^+ blocker. In addition, intracellular K^+

was replaced by 180 mM NMDG. Na^+ channels were blocked with 1 μM TTX. Currents isolated in this way were completely blocked by 200–400 μM Cd^{2+} (Fig. 1f) in this way, and for simplicity, we will refer to these currents as Ca^{2+} currents. Current–voltage relationships (I–V plots) were generated before and after drug application. Figure 1c shows representative Ca^{2+} currents evoked with 20 ms rectangular voltage commands from -80 to 50 mV in 10 mV steps. Figure 1d shows a representative Ca^{2+} current in response to a voltage ramp command (0.7 mV/ms) from -80 to 50 mV. When I–V plot from both methods coincide, space-clamp was considered acceptable (Fig. 1e). For clarity, most figures only show representative responses to voltage ramps.

Current clamp recordings in slices

Current clamp recordings were performed with the patch clamp technique in the whole cell configuration of PV+



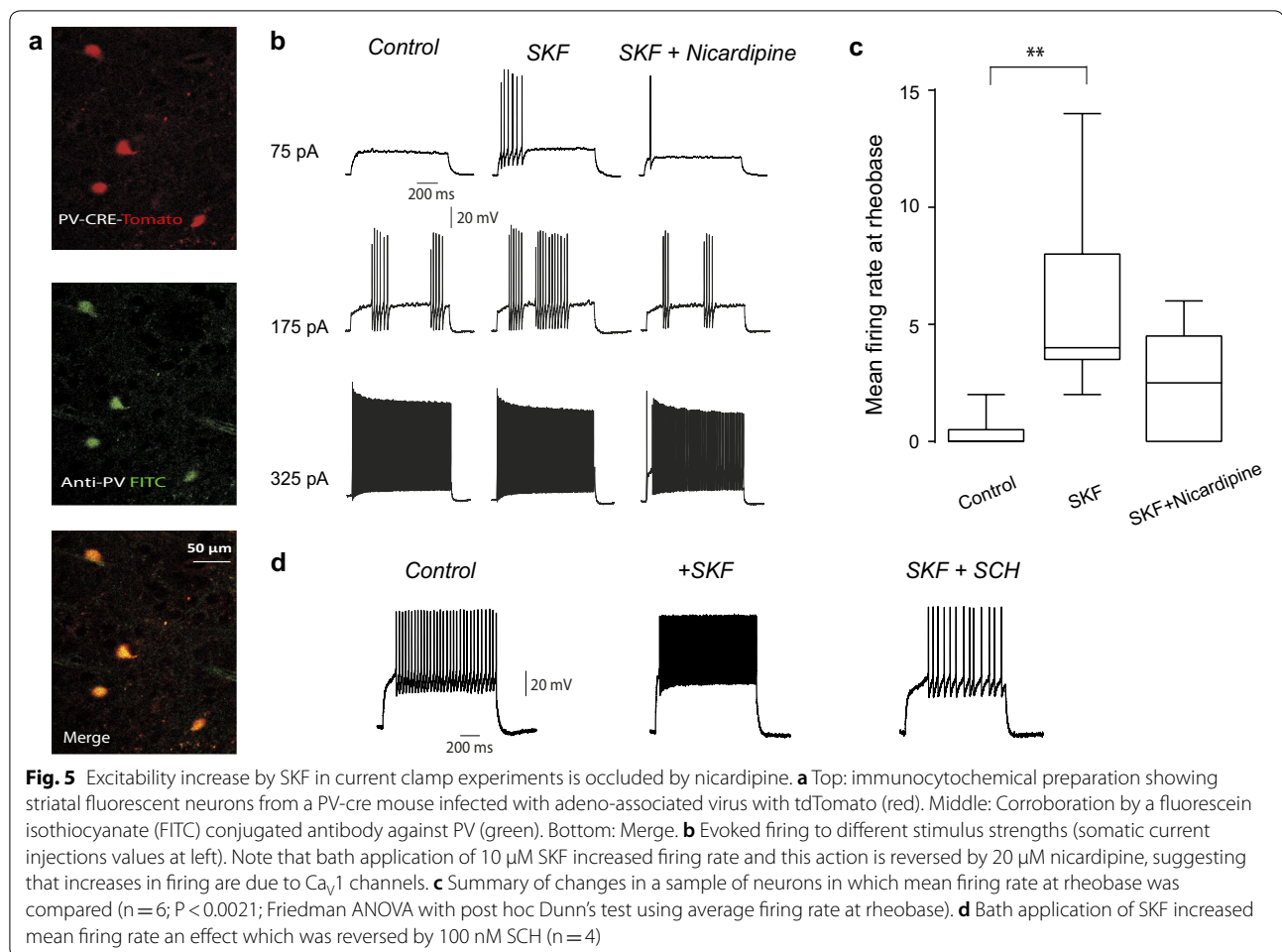
neurons of infected mice ranging in age 28–60 days. Sagittal slices (250–300 μ m thick) were cut using a vibratome (1000 Classic, Warner Instruments, Hamden, USA), transferred to a recording chamber and superfused continuously with oxygenated saline solution (5 ml/min) at room temperature (~ 25 $^{\circ}$ C). Neurons within the striatum

were visualized with infrared differential interference contrast videomicroscopy and PV+ neurons were identified using epifluorescent illumination with a 40 \times immersion objective (0.8 NA; Nikon Instruments, Melville, NY). Micropipettes were pulled (Sutter Instrument, Novato, CA) from borosilicate glass tubes (WPI, Sarasota, FL) to an outer diameter of 1.5-mm for a final D.C. resistance of 4–6 M Ω when filled with internal saline. The internal solution contained (in mM): 120 KSO₃CH₄, 10 NaCl, 10 EGTA, 10 HEPES, 0.5 CaCl₂, 2 MgCl₂, 2 ATP-Mg, and 0.3 GTP-Na (pH=7.3, 290 mOsM/l). Recordings were made with an Axopatch 200A amplifier (Axon Instruments, Foster City, CA) and data were acquired with the Im-Patch[©] software designed in the Lab View environment (freely available for download at im-patch.com). Evoked firing responses at different depolarizing membrane potentials were obtained before and after a selective dopamine receptor agonist was administered. Current–voltage relationships made in current-clamp mode superimposed tightly with those performed in voltage-clamp mode at steady state, suggesting that neither bridge balance, nor series resistance, represented a problem in our recordings.

Digitalized electrophysiological data were imported and analyzed into Origin v8, Microcal (Northampton, MA), and MatLab (The Mathworks Inc. Natick, MA). Data are presented as the mean \pm standard error (SEM). Firing rate plots were made by taking firing rate at rheobase in the different pharmacological conditions (Fig. 5c). Free-distribution statistical tests Wilcoxon’s *T* test and Friedman, one-way ANOVA with post hoc Dunn’s tests were used to assess statistical significance between paired or unpaired samples comparisons. Statistical significance was defined by P-values below 0.05.

Calcium imaging recordings

Calcium imaging recordings were obtained from PV+ neurons of mice infected with a Cre-dependent GCamp6f expression. Recordings were performed in saline solution containing (in mM): 126 NaCl, 2.5 KCl, 26 NaHCO₃, 1.2 NaHPO₄, 1 CaCl₂, 1.3 MgCl₂, 10 glucose, 0.2 thio-urea and 0.2 of ascorbic acid (25 $^{\circ}$ C; pH: 7.4 with HCl, 300 \pm 5 mOsM/l with glucose; saturated with 95% O₂ and 5% CO₂). For recordings, a microscope equipped with a 20 \times 0.95 NA water-immersion objective (XLUMPlanFI, Olympus, Center Valley, PA) which has an image field of 750 \times 750 μ m, was used. To observe spontaneous changes in GCamp6f fluorescence intensity, light pulses at 488 nm (15–50 ms exposure) were delivered to the preparation with a Lambda LS illuminator (Sutter instruments, Petaluma, CA) connected to the microscope via optic fiber. Brief image sequences or movies (~ 180 s per epoch) were acquired with open access Im-Patch[©] software [6] at



time intervals of 5–10 min during ≥ 60 min with a cooled digital camera (CoolSnap K4, Photometrics, Tucson, AZ) and 100–250 ms/image frame. Ca^{2+} entry was seen as spontaneous neuronal intrasomatic Ca^{2+} transients in PV+ neurons whose first time derivative reflects the time of electrical activity [36]. Activity of each cell was illustrated as dots in a raster plot.

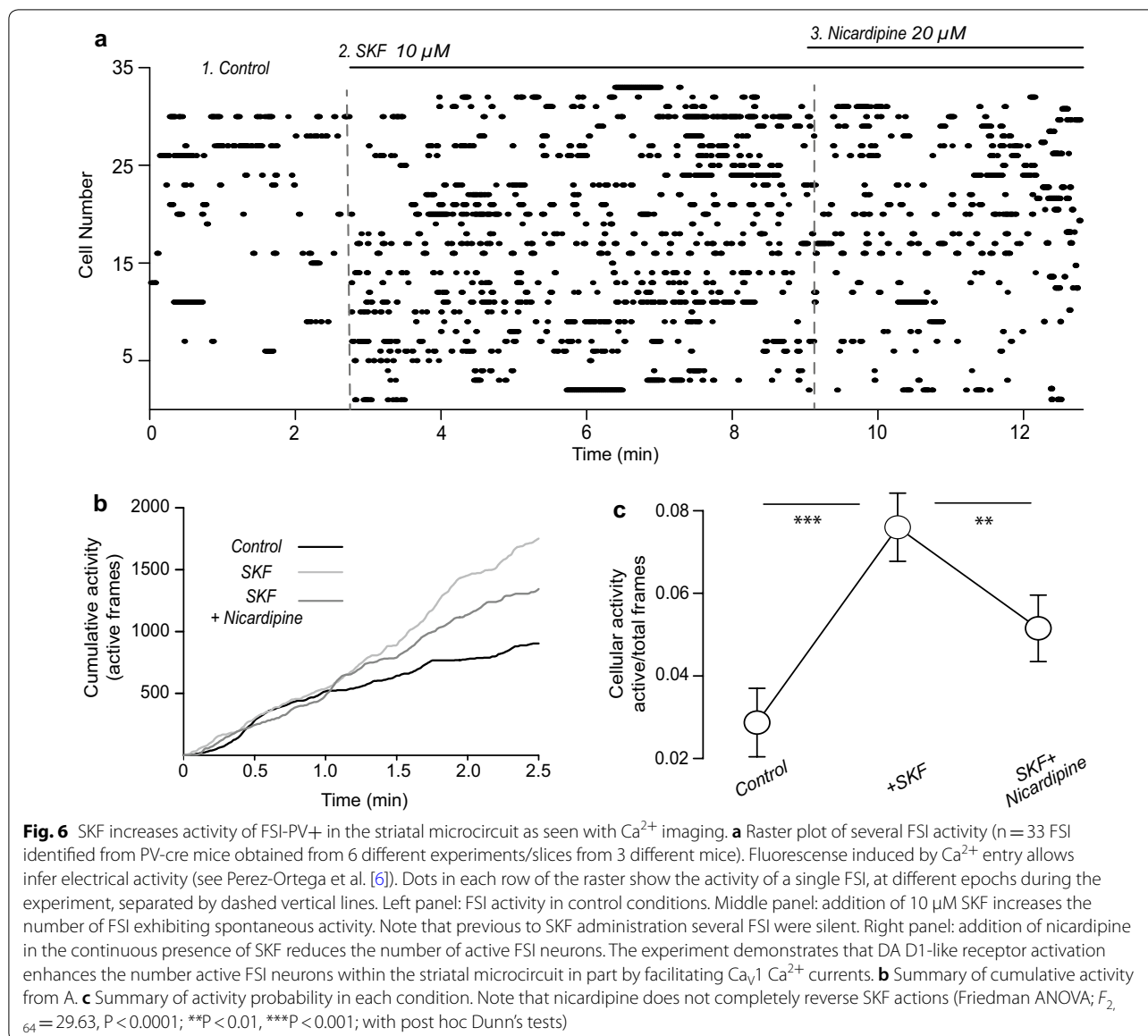
Immunocytochemical procedures

PV-Cre mice were infected as described earlier. Mice were deeply anesthetized (see above) and perfused transcardially with a solution of 4% paraformaldehyde in PBS. Thereafter, animals were decapitated and their brains removed from the skull and fixed overnight with 4% paraformaldehyde in PBS. The brains were then cut on a vibratome into 40 μ m slices that were incubated 30 min with 1% bovine albumina to block nonspecific binding sites and for 36 h with a rabbit polyclonal antibody against parvalbumin (anti PV 1:2000 Abcam dissolved in PBS containing 0.25% Triton-X). The slices were then rinsed thrice with PBS and incubated with a goat versus

rabbit secondary antibody (1:200 Vector Laboratories, Burlingame, CA, dissolved in PBS containing 0.25% Triton-X) during 1 h. This antibody was conjugated with FITC (Vector Laboratories, Burlingame, CA). Samples were mounted with vectashield (Vector Laboratories, Burlingame, CA) and observed in a confocal microscope ZEISS LSM 700 (10 \times /1.0 NA) ($n = 10$).

Drugs

For dissociated cell recordings, drugs were applied with a gravity-fed system that positioned a glass capillary tube 100 μ m from the recording cell in the direction of superfusion flow. Solution changes were performed with a D.C. controlled microvalve system (Lee; Essex, CT, USA). This method allowed reversible drug applications [26, 33]. For current clamp recordings drugs were administered into the bath saline. Substances used were the DA receptor D1-like selective agonist SKF 81297 (Cat# S143), DA receptor D1-like antagonist SCH 23390 (Cat# 125941-87-9), Ca^{2+} Ca_v1 antagonist nicardipine (Cat# N7510) all from Sigma-Aldrich-RBI (St Louis, MO, USA); Ca^{2+}



Ca_v2.2 blocker ω-conotoxin GVIA (Cat# C-300), Ca²⁺ Ca_v3 blocker TTA-P2 (Cat# T-155), Ca²⁺ Ca_v2.3 blocker SNX-482 (Cat# RTS-500), Na⁺ blocker tetrodotoxin (TTX) (Cat# T-550) from Alomone Laboratories (Israel) and Ca²⁺ Ca_v2.1 blocker ω-agatoxin TK (Cat# 4294-s) from Peptides International (Louisville, KY).

Data analysis

Collected digitalized data were analyzed and plotted using commercial software (Origin v8, Microcal, Northampton, MA, USA; RIDD: rid_000069). We report mean ± SEM of peak Ca²⁺ currents changes for dissociated FSI recordings without assuming normal distributions. We also used the 5, 25, 50 (median), 75

and 95 percentile ranges of absolute current values represented as Tukey box plots. Friedman, Kruskal–Wallis or Wilcoxon test with post hoc Dunn for multiple comparisons tests were used (signaled in each Result). Friedman and Wilcoxon test were used when we compared the same samples in two or three different conditions (before, during and after application of a drug). P < 0.05 was used as significance threshold. Analysis was conducted by GraphPad Prism 6.01 (La Joya, CA). Here, Ba²⁺ currents are reported as Ca²⁺ currents and graphs summarizing sampling results are illustrated. For current clamp recordings, we report mean ± SEM of firing rate. For calcium imaging experiments, activity of each FSI was determined as the total number of

active frames/total number of frames. Finally, to quantify the amount of activity on each experiment, a cumulative activity plot was built on each condition.

Contribution of each class of Ca²⁺ channel to the whole-cell Ca²⁺ current

The method to obtain the average contribution of a given class of Ca²⁺ channel to the whole cell Ca²⁺ current was described in previous work [37]. Briefly, to approximate the contribution of each class of Ca²⁺ channel, the amount of Ca²⁺ current blocked by a given antagonist: nicardipine, ω -conotoxin GVIA (ω -CgTx), ω -agatoxin TK (ω -AgTx), TTA-P2 (TTA) and SNX-482 (SNX) was obtained by subtraction in the same or different experiments. Hardly all antagonists could be tested in a single experiment, but the amount blocked by each antagonist was taken no matter the number or order of the antagonists tested. This amount of blocked current was defined as the contribution of that specific channel class to the whole-cell control Ca²⁺ current normalized to 100% without any antagonist. Thereafter the data was introduced in the following system of linear equations:

$$\begin{aligned} 0_{X1} + N_{X2} + PQ_{X3} + T_{X4} + R_{X5} &= A \\ L_{X1} + 0_{X2} + PQ_{X3} + T_{X4} + R_{X5} &= B \\ L_{X1} + N_{X2} + 0_{X3} + T_{X4} + R_{X5} &= C \\ L_{X1} + N_{X2} + PQ_{X3} + 0_{X4} + R_{X5} &= D \\ L_{X1} + N_{X2} + PQ_{X3} + T_{X4} + 0_{X5} &= E \end{aligned}$$

where *L*, *PQ*, *N*, *T* and *R* are the contributions in percentage (\pm SEM) of each channel class: Ca_v1, Ca_v2.2, Ca_v2.1, Ca_v3 and Ca_v2.3 to the whole-cell Ca²⁺ current. For example, PQ refers to the current blockade by the selective P/Q type Ca²⁺ channel antagonist (ω -AgTx). Zero in the linear equation system means a blockade of a given Ca²⁺ channel class, thus, coefficients *L*, *N*, *PQ*, *T* or *R* were replaced by zero when the corresponding Ca²⁺ channel class was blocked. *A*, *B*, *C*, *D* or *E* stand for the mean percentage of Ca²⁺ current in the control (100%) with one channel class blocked (<100%). Subscripts *X1*–*X5* are the unknown variables, in other words, the values that multiply the coefficients *L*, *N*, *PQ*, *T* and *R* in order to determine percentage contribution of each channel to the whole-cell Ca²⁺ current.

Results

Striatal FSI express the Ca²⁺ binding protein PV [2, 38] and activation of the D5-type DA receptor from the D1-like class depolarizes FSI neurons to increase their action potentials (APs) firing rate [20, 21]. However, a final effector and whether DA enhances or decreases Ca²⁺ currents in FSI is unknown. With the help of PV-Cre transgenic mice we explored whether DA receptor

actions in acutely dissociated striatal FSI modulate Ca²⁺ currents. In our experiments Na⁺ and K⁺ channels were blocked (Fig. 1c, d).

Ca²⁺ channels expressed in striatal FSI

FSI were identified using mice expressing Cre-recombinase under the control of the PV promoter (PV-Cre) and stereotaxic injections of an adeno-associated virus into the dorsal striatum allowed expression of a fluorescent protein (td-Tomato) only in striatal FSI. Acutely dissociated neurons were used in the first part of this study to avoid any indirect inputs from afferents, gap junctions, dendritic or axonal inputs. First, we estimated which Ca²⁺ channels are present in the soma and nearby dendrites of FSI and their percentage contribution to the overall whole cell Ca²⁺ current optimizing space clamp (Fig. 1e and current isolation; see Methods). Ca²⁺ entry through different calcium channels exert different and complex responses that vary in different cell types and localization within the cell body [37 for a review], therefore, one goal of this study was to determine the classes of voltage gated Ca²⁺ channels present in striatal FSI. Representative experiments with time courses of Ca²⁺ current amplitudes before and after application of specific channels antagonists is shown in Fig. 2a, b and percentage contribution of each Ca²⁺ channel class is summarized in Table 1. Antagonists were administered in different order or alone, and the current they reduced was compared with the whole cell Ca²⁺ current without any antagonist (see Methods). To determine whether Ca_v1 (L-type) contributed to the whole-cell current, application of nicardipine, a specific Ca_v1 Ca²⁺ channels antagonist was examined. As shown in Fig. 2a, nicardipine at saturating concentrations (20 μ M) reduces whole-cell current amplitude by $38 \pm 1.1\%$. This reduction was significant when whole cell current was normalized to 100% for the current without any antagonist in control conditions ($n = 12$; $P = 0.0001$; Kruskal–Wallis ANOVA with post hoc Dunn's test, used in this and next antagonists cases, percentages were obtained with the system of linear equations described in the Methods and compared to whole cell Ca²⁺ current without any drugs). This large amount of current flux through Ca_v1 Ca²⁺ channel might contribute to neuronal depolarization and AP generation after addition of D1-like agonist, since this current have a slow voltage-dependent inactivation [20, 25, 39, 40]; a main hypothesis tested below.

Ca_v2.2 (N) contribute to $23.4 \pm 0.7\%$ as revealed by 1 μ M of ω -conotoxin GVIA (ω -CgTx) blockade, a specific Ca_v2.2 channel antagonist (Fig. 2a, Table 1; $P = 0.0001$; $n = 14$). Contribution of Ca_v2.1 (P/Q) was $11.1 \pm 1.4\%$ disclosed by ω -agatoxin TK (1 μ M; Fig. 2a; Table 1; $P = 0.0033$). 1 μ M SNX-482 revealed the presence of

Table 1 Contribution in percentage of the whole-cell Ca²⁺ current for each class of Ca²⁺ channel

Antagonist	Nicardipine	ω -conotoxin GVIA	ω -Agatoxin TK	SNX-482	TTA-P2
Concentration	20 μ M	1 μ M	1 μ M	1 μ M	1 μ M
Ca ²⁺ channel antagonist	Ca _v 1	Ca _v 2.2	Ca _v 2.1	Ca _v 2.3	Ca _v 3
% of current blocked (mean \pm S.E.M)	38 \pm 1.1	23.4 \pm 0.7	11.1 \pm 1.4	20 \pm 2	7.4 \pm 2.3
n	12	14	14	6	13
p	0.0001	0.0001	0.0033	0.0009	0.0202

The first row (not counting the title) indicates the Ca²⁺ channel antagonist used. The second row contains saturating concentrations used. Third row stands for the specific Ca²⁺ channel class that was blocked. The fourth row displays the mean \pm SEM of Ca²⁺ current blocked in percentage by each antagonist. Antagonists were tested alone or in sequence in different orders. Percentages were obtained from a system of linear equations that used data from all experiments (see Materials and methods). The fifth row shows samples size: the number of neurons tested with each antagonist. The sixth row indicates statistical significance or P-value of percentage blockade by each antagonist as compared to whole-cell current average before adding any antagonist (Kruskal–Wallis ANOVA with post hoc Dunn's test of each paired comparison against the control: whole-cell Ca²⁺ current)

Ca_v2.3 (R) Ca²⁺ channels: 20 \pm 2% (Fig. 2b; Table 1; n = 6; P = 0.0009). Finally, Ca_v3 (T) Ca²⁺ channels contribute with 7.4 \pm 2.3% (Fig. 2b; Table 1; n = 13; P = 0.0202). To conclude, representative components of high voltage gated (HVA) and low voltage gated (LVA) Ca²⁺ channels are present in FSI. The specific type and role of each of these channels is a matter of future studies out of the scope of the present work. We next concentrate on Ca_v1 Ca²⁺ channels which provide much of the whole cell Ca²⁺ current.

Activation of D1-class receptor enhances Ca²⁺ currents in acutely dissociated FSI

To know whether DA has effect on FSI Ca²⁺ currents, we performed whole-cell recordings in dissociated and identified FSI cells. Time course of peak current is shown in I–V plots of Fig. 3a before, during and after the administration of 10 μ M of the DA receptor D1-like agonist SKF-81297 (SKF). SKF enhanced whole-cell Ca²⁺ currents in all FSI tested by an average of 34 \pm 14% (Fig. 3a, b; n = 8. Friedman ANOVA test $F_{2,14} = 13$, P = 0.0003; *P < 0.05, **P < 0.01; with post hoc Dunn's test). Note that Ca²⁺ current returns to values similar to the control when the agonist is washed-off. Representative I–V plots (Fig. 3a right) are shown at different moments of the time course. Box plot in Fig. 3b summarizes the results from the previous sample of experiments showing that SKF actions were significant. The effect of the SKF was blocked by the presence of 100 nM of the DA receptor D1-like antagonist SCH 23390 (SCH; Fig. 3c). Removal of SCH leads to an increase in Ca²⁺ current in the presence of SKF showing that activation of D1-like DA receptors, most probably D5 [20, 21], enhances Ca²⁺ currents in FSI. No significant differences were found comparing controls and the combination SCH/SKF (Fig. 3d) (n = 8; Wilcoxon T test P > 0.9999). These results are consistent with the expression of D1-class DA receptors in FSI and show that DA

enhances Ca²⁺ currents through the activation of these receptors.

D1-like receptors modulate Ca_v1 Ca²⁺ channel current

To further investigate the role of DA on Ca²⁺ currents we performed experiments blocking Ca²⁺ currents while activating DA receptors. Because Ca_v1 Ca²⁺ channels provide the most to the whole cell Ca²⁺ current we first blocked them [25]. Time course of peak current amplitude (top) and a representative I–V plots (bottom) are illustrated in Fig. 4a showing first, the action of 20 μ M of the selective antagonist nicardipine on Ca_v1 currents. Then the action of subsequent application of the D1-like agonist SKF is shown. Nicardipine reduced Ca²⁺ current by 55.4 \pm 7.8% in this sample (Fig. 4a, b; n = 8; Friedman ANOVA test $F_{2,14} = 13$, P = 0.0003; *P < 0.05, **P < 0.01 with post hoc Dunn's test). Note that in the presence of nicardipine subsequent addition of 10 μ M SKF fail to elicit any change in the remaining Ca²⁺ current (P = 0.9999; Dunn's test). We conclude that the action of nicardipine occluded the action of SKF and therefore Ca_v1 Ca²⁺ channels are the final effectors of DA receptor modulation; without excluding other classes of channels (Na⁺, K⁺). This action is similar to that found in striatonigral projection neurons expressing D1-like receptors in both cell bodies and terminals [15, 41, 42]. It is also inferred that with respect to Ca²⁺ currents, there is no other effector for D1- receptor modulation in FSI.

D1-like receptors enhance FSI firing rate by modulating Ca_v1 Ca²⁺ channels

We then asked whether Ca_v1 Ca²⁺ channels modulation is robust enough to explain, in part, the increase in firing rate due to D1-like receptor modulation in FSI [20, 21]. Whole-cell current-clamp experiments on identified PV+ neurons in slices of transfected PV-Cre mice were performed. FSI in the dorsal striatum were identified based on adeno-associated virus containing td-Tomato

(Fig. 5a top left; see Methods) and corroborated with an antibody against PV conjugated to fluorescein isothiocyanate (FITC; Fig. 5a middle left). Merge is at the bottom in Fig. 5a. FSI were also identified by their electrophysiological phenotype: ability to fire at high firing rates with almost no frequency adaptation as well as stuttering (Fig. 5b). Representative recordings evoked by different intracellular current injections are shown in Fig. 5b: 10 μ M SKF induced increases in mean firing rate at rheobase ($n=6$; $P<0.0001$; Friedman ANOVA with post hoc Dunn's test using average firing rate after 300 pA. Fig. 5c). Notably, subsequent administration of the Ca_v1 antagonist, nicardipine (20 μ M), reversed in part the increase in firing rate induced by SKF. The same was true for a D1-receptor antagonist SCH (Fig. 5d; $n=4$). Several seconds had to be taken between stimuli that evoke firing, before and after drugs administration, since in our hands, intensity-frequency plots exhibited hysteresis (adverse effect), a phenomenon that needs further investigation but out of the scope of the present report.

Activation of D1-class receptors enhances FSI activity in the dorsal striatal microcircuit

Finally, we asked whether activation of DA D1-class receptors can enhance the number of active FSI within the striatal microcircuit by enhancing Ca_v1 Ca^{2+} current. To test this hypothesis we performed calcium imaging experiments with single cell resolution [36] in slices from PV-Cre transgenic mice expressing GCaMP6f as a fluorophore. Using this technique we recorded spontaneous calcium transients of several PV+ neurons in different slices from three mice. The time derivative of these calcium transients indicates their firing time [36]. FSI may fire spontaneously in control conditions together with the firing of other striatal neurons. To avoid confounds we only graphed FSI activity using raster plots where dots in each row represent the moments of activity of single neurons (Methods). The firing of FSI from different slices ($n=6$) are plotted together (Fig. 6a) as previously described [6, 36, 43]. Changes in fluorescence were obtained before, during and after application of SKF and SKF plus nicardipine. Raster plot of active FSI during a period of 13 min recording is shown in Fig. 6a ($n=33$ identified FSI). The left panel in Fig. 6a shows the basal FSI activity in the striatal microcircuit without adding any excitatory drive or drug. Notice scarce FSI activity in control conditions. In contrast, administration of 10 μ M SKF to the bath saline increased the number of active FSI (Fig. 6a middle panel). The subsequent addition of nicardipine in the presence of SKF reduced, but not completely reversed the enhanced activity. Figure 6b shows cumulative activity of all FSI neurons along time [43] and Fig. 6c shows activity probability under each

condition (mean \pm SEM). To compare activity over time a cellular activity value for each neuron at each condition was calculated (frames with active neuron/total number of frames). In control conditions cellular activity was 0.03 ± 0.008 , SKF raised activity to 0.07 ± 0.008 (Fig. 6b, c; Friedman ANOVA $F_{2,64}=29.63$, $P<0.0001$; post hoc Dunn's test). This result indicates that DA increases the number of FSI firing within the striatal microcircuit in agreement with data from dissociated neurons and slice experiments. 20 μ M nicardipine (Fig. 6a right panel) reduced FSI activity to 0.05 ± 0.008 (Fig. 6b, c; $P<0.001$, Dunn's test).

Discussion

A summary of original data and findings of the present work follow: (1) all major classes of voltage gated Ca^{2+} channels are present in striatal FSI (Ca_v1 , $Ca_v2.1-3$; Ca_v3). These results were obtained in voltage-clamp mode in identified dissociated FSI. Specific channel subtypes are still in need of investigation. (2) Contributions in percentage of each Ca^{2+} channel class are reported. Ca_v1 channels represent much of the whole cell Ca^{2+} current. (3) DA D1-class receptors, probably D_5 -type [21], up-modulate Ca_v1 carried current. (4) The Ca_v1 class is the only Ca^{2+} channel modulated by DA in FSI. This modulation is occluded by a previous administration of nicardipine or blocked by the antagonist SCH [20]. (5) Modulation of Ca_v1 Ca^{2+} channels is reflected in an increase in firing rate of FSI. These data were obtained in slices in current clamp mode. (6) Ca^{2+} -imaging recordings of several identified FSI obtained from different slices/animals showed that DA increases the number of FSI that are active in the striatal microcircuit. To our knowledge these are the first evidences of a molecular final effector for the DA-dependent modulation in striatal FSI, leading to a better understanding of the DA actions in the striatum.

Ca^{2+} channels expressed in FSI

Using pharmacological tools here we demonstrate that identified FSI from transgenic animals may be isolated in enough number to study the ion channels they express with whole-cell voltage clamp techniques in acutely dissociated preparations, thus eliminating indirect sources or confounds such as inputs from other neurons as well as gap junctions and chemical synapses between FSI themselves, this maneuver allows study specific Ca^{2+} currents [30, 33, 34, 37]. Striatal FSI seem to express all classes of voltage gated Ca^{2+} channels, HVA (Ca_v1 , $Ca_v2.1$, $Ca_v2.2$ and $Ca_v2.3$) and LVA (Ca_v3), although, their contributions vary (Fig. 2a, b and Table 1). On average, Ca_v1 channels contribute the most to the whole cell Ca^{2+} current followed by $Ca_v2.2$ and $Ca_v2.3$ channels

that altogether make up to more than 80% of the whole cell Ca^{2+} current. $\text{Ca}_v2.1$ and Ca_v3 make up the remaining current. Together with other ion channels [44–46], the studied Ca^{2+} channels shape the characteristic firing properties [28, 44–46] of FSI and may be orchestrated by signaling pathways as it occurs in striatal projection neurons (SPNs) [27, 30, 37, 40, 41]. Although it was not the goal of the present study to explore the role of each Ca^{2+} channel encountered, the variety found may imply that each channel has a specific role and ways to be modulated [6, 13, 14, 30, 35, 37, 40, 41]. Pathologies associated with striatal FSI, such as anxiety-like behaviors, schizophrenia or disorders such as Tourette's and Huntington's disease as well as some channelopathies [7, 47–51] may use this preparation to study associated changes.

Dopaminergic modulation of striatal FSI Ca^{2+} currents

A selective D1-class DA receptor agonist, SKF-81297, was used to investigate dopaminergic modulation. The DA receptor agonist enhanced Ca^{2+} currents specifically carried by Ca_v1 channels in FSI. A previous blockade of these channels with a dihydropyridine, nifedipine, completely occluded the action of the DA receptor agonist. Notably, this is similar to the dopaminergic modulation found in direct basal ganglia projection neurons (dSPNs) except that in the present case there was no need to block intracellular phosphatases [20].

Current through Ca_v1 channels has been associated with enhanced evoked depolarization and discharge facilitation [41, 52, 53]. Current clamp experiments in slices showed that this is also the case for striatal FSI as well as other neurons [37]. Ca_v1 also induces short-term synaptic depression and facilitates GABA release in SNr [53, 54]. Blockade of enhanced firing by nifedipine shows that Ca_v1 channels are in part responsible for these functions in striatal FSI. It would be interesting to know if FSI from other nuclei express this modulation or if it is particular for striatal FSI.

In addition, dynamic Ca^{2+} imaging of identified FSI with single cell resolution showed that the firing of these interneurons is enhanced in the striatal microcircuit by dopaminergic modulation. This action was partially blocked by nifedipine, lasted for several minutes without overt desensitization, suggesting that D1-class receptor activation, probably D5-type, increases feed-forward inhibition in the microcircuit [1, 55, 56]. Network analyses of this action in control and disease *in vitro* models [6] deserve further study. In addition, calcium recording was not performed *in vivo*, so the impact of excitatory drive from cortex and thalamus were not evaluated in the DAergic actions reported, although, *in vitro* studies have shown similar suprathreshold responses on thalamic and cortical stimuli, suggesting that both sources produces

similar feed-forward inhibition on SPN [11]. Given that the resonant frequency of FSI is within the gamma band [57], it may be logical to infer that DA modulation favors gamma (Piper) rhythms within neuronal circuits [4, 58–60]. On the other hand, aberrant or excessive gamma rhythms may be present during schizophrenia and L-DOPA induced dyskinesia [8, 18, 61].

However, the number of dopamine activated FSI within the striatal microcircuit does not return to control conditions after Ca_v1 Ca^{2+} channels are blocked. There could be various reasons for this behavior. One is that the DA receptor agonist not only affects FSI within the circuit, but turns on network activity in a way that does not return to control even after blocking Ca_v1 in FSI [19, 62]. Another explanation is that circuit activity or DA activates other ion channels in FSI [19]. Finally, FSI form networks of interconnected neurons both electrically and chemically [1, 2, 11]. This last property may correlate FSI firing making hard to study their individual cell responses in striatal brain slices.

Conclusion

To our knowledge this is the first demonstration that Ca_v1 channels are final effectors of DA modulation in FSI. In addition, we show the classes of Ca^{2+} channels that striatal FSI express and show evidence that Ca_v1 are the only ones modulated by D1-class receptors activation. Enhancement of Ca_v1 channels is a main cause for the increase in excitability of these interneurons due to DA receptors signaling, and collectively, this modulation increases the number of active FSI during striatal microcircuit operation. The demonstration that identified interneurons can be isolated for recording opens the pathway for future studies such as: to study other current classes (K^+ , Na^+) and their modulation in interneurons in space clamp conditions, it also suggests comparisons between current phenotypes between FSIs from the striatum and other nucleus such as the cortex, and finally, quantitative single cell PCR may be used to prove whether different regions of the striatum possess different types of FSIs.

Abbreviations

FSI: fast spiking interneurons; PV: parvalbumin; HVA: high voltage activated; LVA: low voltage activated; SPN: spiny projection neurons; dSPN: striatonigral projection neurons; TTX: tetrodotoxin; SNc: substantia nigra pars compacta; ChAT: giant cholinergic interneurons; DA: dopamine; HEPES: 4-(2-hydroxyethyl)-1-piperazineethanesulfonic acid; NMDG: N-methyl-D-glucamine; eGFP: enhanced green fluorescent protein; iFR: instantaneous firing rate.

Authors' contributions

JB: conception of research. EAR-O, TH-F, VHA-R and JB: designed the isolated neurons and current clamp experiments. EAR-O, TH-F and VHA-R: performed isolated neuron electrophysiology experiments. MD and AL: performed, analyzed, interpreted and reported calcium imaging experiments. EAR-O,

VAC-C: performed and analyzed current clamp experiments. AL: performed analytical code to obtain the contribution of Ca^{2+} channels. EAR-O, MD, VAC-C, VHA-R and TH-F: performed mice transfections. DT and EG: performed and analyzed immunocytochemical experiments. EAR-O, VHA-R, VAC-C, AL, DT, EG and JB: interpreted and analyzed data. EAR-O and JB: wrote the manuscript. All authors participated actively with important experimental and intellectual content to the design, content, analysis, discussion and conclusions of the study. All authors read and approved the final manuscript.

Acknowledgements

Gabriela X Ayala and Ariadna Aparicio-Júarez for technical support and advice and to Dr. Claudia Rivera for animal care. A. Luna collaborated in some experiments.

Competing interests

The authors declare they have no competing interests.

Availability of data and materials

All datasets and/or analyses used in this study are available in the laboratory server which cannot be public as a whole, since it contains data from several works. However, data from this work can be made available from the corresponding author upon a reasonable request.

Consent for publication

Not applicable.

Ethical approval and consent to participate

No human subjects or material was employed in this work. All experiments were carried out in accordance with the Mexican technical specifications for the production, care and use of laboratory animals (NOM-062-ZOO-1999), the National Institutes of Health guide for the care and use of Laboratory animals (NIH Publications No. 8023, revised 1978 and 2010) and was approved by the Institutional Committee for Laboratory Animals Care and Use of the Instituto de Fisiología Celular (IFC; UNAM, FTA03-14; laboratory procedures common to several projects JBD-59-15); minimizing the number of animals to achieve statistical significance and avoiding animal suffering.

Funding

This work was supported by Grants from Consejo Nacional de Ciencia y Tecnología, Mexico (CONACyT, 251144 to EG and Frontera 57 to JB) and from Dirección General de Asuntos del Personal Académico, Universidad Nacional Autónoma de México (DGAPA-UNAM) IN201517 to EG and IN201417 to JB. After funding approval, funding institutions had no role in the design, collection, analyses, interpretation of data and writing of the manuscript. In addition, Ernesto Alberto Rendón-Ochoa had a CONACyT doctoral fellowship: 261720. Data in this work are part of his doctoral dissertation in the Programa de Maestría y Doctorado en Ciencias Bioquímicas, Facultad de Química, Universidad Nacional Autónoma de México.

Publisher's Note

Springer Nature remains neutral with regard to jurisdictional claims in published maps and institutional affiliations.

Received: 5 April 2018 Accepted: 7 July 2018

Published online: 16 July 2018

References

- Koós T, Tepper JM. Inhibitory control of neostriatal projection neurons by GABAergic interneurons. *Nat Neurosci*. 1999;2(5):467–72.
- Koós T, Tepper JM. Dual cholinergic control of fast-spiking interneurons in the neostriatum. *J Neurosci*. 2002;22(2):529–35.
- Ramanathan S, Hanley JJ, Deniau JM, Bolam JP. Synaptic convergence of motor and somatosensory cortical afferents onto GABAergic interneurons in the rat striatum. *J Neurosci*. 2002;22(18):8158–69.
- Sohal VS, Zhang F, Yizhar O, Deisseroth K. Parvalbumin neurons and gamma rhythms enhance cortical circuit performance. *Nature*. 2009;459(7247):698–702.
- Berke JD. Functional properties of striatal fast-spiking interneurons. *Front Syst Neurosci*. 2011;5(45):1–7.
- Pérez-Ortega J, Duhne M, Lara-González E, Plata V, Gasca D, Galarraga E, Hernández-Cruz A, Vargas J. Pathophysiological signatures of functional connectomics in parkinsonian and dyskinetic striatal microcircuits. *Neurobiol Dis*. 2016;91:347–61.
- Xu M, Li L, Pittenger C. Ablation of fast-spiking interneurons in the dorsal striatum, recapitulating abnormalities seen post-mortem in Tourette syndrome, produces anxiety and elevated grooming. *Neuroscience*. 2016;324:321–9.
- Yamada H, Inokawa H, Hori Y, Pan X, Matsuzaki R, Nakamura K, Samejima K, Shisara M, Kimura M, Sakagami M, Minamimoto T. Characteristics of fast-spiking neurons in the striatum of behaving monkeys. *Neurosci Res*. 2016;105:2–18.
- Tepper JM, Tecuapetla F, Koós T, Ibáñez-Sandoval O. Heterogeneity and diversity of striatal GABAergic interneurons. *Front Neuroanat*. 2010;4(150):1–18.
- Reig R, Silberberg G. Multisensory integration in the mouse striatum. *Neuron*. 2014;83(5):1200–12.
- Arias-García MA, Tapia D, Laville JA, Calderón VM, Ramiro-Cortés Y, Vargas J, Galarraga E. Functional comparison of corticostriatal and thalamostriatal postsynaptic responses in striatal neurons of the mouse. *Brain Struct Funct*. 2018;223(3):1229–53.
- Gittis AH, Leventhal DK, Fensterheim BA, Pettibone JR, Berke JD, Kreitzer AC. Selective inhibition of striatal fast-spiking interneurons causes dyskinesias. *J Neurosci*. 2011;31(44):15727–31.
- Damodaran S, Evans RC, Blackwell KT. Synchronized firing of fast-spiking interneurons is critical to maintain balanced firing between direct and indirect pathway neurons of the striatum. *J Neurophysiol*. 2014;111(4):836–48.
- Surmeier DJ, Vargas J, Hemmings HC, Nairn AC, Greengard P. Modulation of calcium currents by a D1 dopaminergic protein kinase/phosphatase cascade in rat neostriatal neurons. *Neuron*. 1995;14:385–97.
- Bolam JP, Hanley JJ, Booth PA, Bevan MD. Synaptic organization of the basal ganglia. *J Anat*. 2000;196:527–42.
- Gerfen CR, Surmeier DJ. Modulation of striatal projection systems by dopamine. *Annu Rev Neurosci*. 2011;34:441–66.
- Surmeier DJ, Carrillo-Reid L, Vargas J. Dopaminergic modulation of striatal neurons, circuits, and assemblies. *Neuroscience*. 2011;198:3–18.
- Tritsch NX, Sabatini BL. Dopaminergic modulation of synaptic transmission in cortex and striatum. *Neuron*. 2012;76(1):33–50.
- Carrillo-Reid L, Hernández-López S, Tapia D, Galarraga E, Vargas J. Dopaminergic modulation of the striatal microcircuit: receptor-specific configuration of cell assemblies. *J Neurosci*. 2011;31(42):14972–83.
- Bracci E, Centonze D, Bernardi G, Calabresi P. Dopamine excites fast-spiking interneurons in the striatum. *J Neurophysiol*. 2002;87(4):2190–4.
- Centonze D, Grande C, Usiello A, Gubellini P, Erbs E, Martin AB, Pisani A, Tognazzi N, Bernardi G, Moratalla R, Borrelli E, Calabresi P. Receptor subtypes involved in the presynaptic and postsynaptic actions of dopamine on striatal interneurons. *J Neurosci*. 2003;23(15):6245–54.
- Gorelova N, Seamans JK, Yang CR. Mechanisms of dopamine activation of fast-spiking interneurons that exert inhibition in rat prefrontal cortex. *J Neurophysiol*. 2002;88(6):3150–66.
- Kröner S, Krimer LS, Lewis DA, Barrionuevo G. Dopamine increases inhibition in the monkey dorsolateral prefrontal cortex through cell type-specific modulation of interneurons. *Cereb Cortex*. 2007;17(5):1020–32.
- Kröner S, Rosenkranz JA, Grace AA, Barrionuevo G, Kro S. Dopamine modulates excitability of basolateral amygdala neurons in vitro dopamine. *J Neurophysiol*. 2005;93(3):1598–610.
- Pérez-García E, Vargas J, Galarraga E. The role of Ca^{2+} channels in the repetitive firing of striatal projection neurons. *NeuroReport*. 2003;14(9):1253–6.
- Perez-Rosello T, Figueroa A, Salgado H, Vilchis C, Tecuapetla F, Guzman JN, Galarraga E, Vargas J. Cholinergic control of firing pattern and neurotransmission in rat neostriatal projection neurons: role of $Ca_v2.1$ and $Ca_v2.2$ Ca^{2+} channels. *J Neurophysiol*. 2005;93(5):2507–19.
- Vargas J, Ayala GX, Vilchis C, Pineda JC, Galarraga E. Ca^{2+} -activated outward currents in neostriatal neurons. *Neuroscience*. 1999;88(2):479–88.
- Bennett BD, Callaway JC, Wilson CJ. Intrinsic membrane properties underlying spontaneous tonic firing in neostriatal cholinergic interneurons. *J Neurosci*. 2000;20(22):8493–503.

29. Chen TW, Wardill TJ, Sun Y, Pulver SR, Renninger SL, Baohan A, Schreier ER, Kerr RA, Orger MB, Jayaraman V, Loofer LL, Svoboda K, Kim DS. Ultrasensitive fluorescent proteins for imaging neuronal activity. *Nature*. 2013;499(7458):295–300.
30. Bargas J, Howe A, Eberwine J, Cao Y, Surmeier DJ. Cellular and molecular characterization of Ca²⁺ currents in acutely isolated, adult rat neostriatal neurons. *J Neurosci*. 1994;14(11):6667–86.
31. Perez-Burgos A, Perez-Rosello T, Salgado H, Flores-Barrera E, Prieto GA, Figueroa A, Galarraga E, Bargas J. Muscarinic M1 modulation of N and L types of calcium channels is mediated by protein kinase C in neostriatal neurons. *Neuroscience*. 2008;155(4):1079–97.
32. Perez-Burgos A, Prieto GA, Galarraga E, Bargas J. Ca_v2.1 channels are modulated by muscarinic M1 receptors through phosphoinositide hydrolysis in neostriatal neurons. *Neuroscience*. 2010;165(2):293–9.
33. Hernández-González O, Hernández-Flores T, Prieto GA, Pérez-Burgos A, Arias-García MA, Galarraga E, Bargas J. Modulation of Ca²⁺-currents by sequential and simultaneous activation of adenosine A1 and A2A receptors in striatal projection neurons. *Purinergic Signal*. 2014;10(2):269–81.
34. Hernández-Flores T, Hernández-González O, Pérez-Ramírez MB, Lara-González E, Arias-García MA, Duhne M, Pérez-Burgos A, Prieto GA, Figueroa A, Galarraga E, Bargas J. Modulation of direct pathway striatal projection neurons by muscarinic M4-type receptors. *Neuropharmacology*. 2015;89:232–44.
35. Bargas J, Surmeier DJ, Kitai ST. High- and low-voltage activated calcium currents are expressed by neurons cultured from embryonic rat neostriatum. *Brain Res*. 1991;541(1):70–4.
36. Carrillo-Reid L, Tecuapetla F, Tapia D, Hernández-Cruz A, Galarraga E, Drucker-Colin R, Bargas J. Encoding network states by striatal cell assemblies. *J Neurophysiol*. 2008;99(3):1435–50.
37. Vilchis C, Bargas J, Pérez-Roselló T, Salgado H, Galarraga E. Somato-statin modulates Ca²⁺ currents in neostriatal neurons. *Neuroscience*. 2002;109(3):555–67.
38. Kawaguchi Y, Wilson CJ, Augood SJ, Emson PC. Striatal interneurons: chemical, physiological and morphological characterization. *Trends Neurosci*. 1995;18(12):527–35.
39. Catterall WA. Voltage-gated calcium channels. *Cold Spring Harb Perspect Biol*. 2011;3(8):1–23.
40. Hernandez-Lopez S, Tkatch T, Perez-Garci E, Galarraga E, Bargas J, Hamm H, Surmeier DJ. D2 dopamine receptors in striatal medium spiny neurons reduce L-type Ca²⁺ currents and excitability via a novel PLCβ1-IP3-calcineurin-signaling cascade. *J Neurosci*. 2000;20(24):8987–95.
41. Hernandez-Lopez S, Bargas J, Surmeier DJ, Reyes A, Galarraga E. D1 receptor activation enhances evoked discharge in neostriatal medium spiny neurons by modulating an L-type Ca²⁺ conductance. *J Neurosci*. 1997;17(9):3334–42.
42. Guzmán JN, Hernández A, Galarraga E, Tapia D, Laville A, Vergara R, Aceves J, Bargas J. Dopaminergic modulation of axon collaterals interconnecting spiny neurons of the rat striatum. *J Neurosci*. 2003;23(26):8931–40.
43. Plata V, Duhne M, Pérez-Ortega JE, Barroso-Flores J, Galarraga E, Bargas J. Direct evaluation of L-DOPA actions on neuronal activity of parkinsonian tissue in vitro. *Biomed Res Int*. 2013;519184:1–7.
44. Rudy B, McBain CJ. Kv3 channels: voltage-gated K⁺ channels designed for high-frequency repetitive firing. *Trends Neurosci*. 2001;24(9):517–26.
45. Erisir A, Lau D, Rudy B, Leonard CS. Function of specific K⁺ channels in sustained high-frequency firing of fast-spiking neocortical interneurons. *J Neurophysiol*. 1999;82(5):2476–89.
46. Lenz S, Perney TM, Qin Y, Robbins E, Chesselet MF. GABA-ergic interneurons of the striatum express the Shaw-like potassium channel Kv3.1. *Synapse*. 1994;18(1):55–66.
47. Cepeda C, Galvan L, Holley SM, Rao SP, André VM, Botelho EP, Chen JY, Watson JB, Deisseroth K, Levine MS. Multiple sources of striatal inhibition are differentially affected in Huntington's disease mouse models. *J Neurosci*. 2013;33(17):7393–406.
48. Rossignol E, Urbani A, Pietrobon D. Role of different voltage-gated Ca²⁺ channels in cortical spreading depression: specific requirement of P/Q-type Ca²⁺ channels. *Channels*. 2011;5(2):110–4.
49. Tottene A, Urbani A, Pietrobon D. Role of different voltage-gated Ca²⁺ channels in cortical spreading depression: specific requirement of P/Q-type Ca²⁺ channels. *Channels*. 2011;5(2):110–4.
50. Kataoka Y, Kalanithi PS, Grantz H, Schwartz ML, Saper C, Leckman JF, Vaccarino FM. Decreased number of parvalbumin and cholinergic interneurons in the striatum of individuals with Tourette syndrome. *J Comp Neurol*. 2010;518(3):277–91.
51. Kalanithi PS, Zheng W, Kataoka Y, DiFiglia M, Grantz H, Saper CB, Schwartz ML, Leckman JF, Vaccarino FM. Altered parvalbumin-positive neuron distribution in basal ganglia of individuals with Tourette syndrome. *Proc Natl Acad Sci USA*. 2005;102(37):13307–12.
52. Galarraga E, Hernández-López S, Reyes A, Barral J, Bargas J. Dopamine facilitates striatal EPSPs through an L-type Ca²⁺ conductance. *NeuroReport*. 1997;889(10):2183–6.
53. Tecuapetla F, Carrillo-Reid L, Bargas J, Galarraga E. Dopaminergic modulation of short-term synaptic plasticity at striatal inhibitory synapses. *Proc Natl Acad Sci USA*. 2007;104(24):10258–63.
54. Recillas-Morales S, Sanchez-Vega L, Ochoa-Sanchez N, Caballero-Floran I, Paz-Bermudez F, Silva I, Aceves J, Erlj D, Floran B. L-type Ca²⁺ channel activity determines modulation of GABA release by dopamine in the substantia nigra reticulata and the globus pallidus of the rat. *Neuroscience*. 2014;256:292–301.
55. Tepper JM, Wilson CJ, Koós T. Feedforward and feedback inhibition in neostriatal GABAergic spiny neurons. *Brain Res Rev*. 2008;58:272–81.
56. Wang W, Nitulescu I, Lewis JS, Lemos JC, Bamford IJ, Posielski NM, Storey GP, Phillips PE, Bamford NS. Overinhibition of corticostriatal activity following prenatal cocaine exposure. *Ann Neurol*. 2013;73:355–69.
57. Beatty JA, Song SC, Wilson CJ. Cell-type-specific resonances shape the responses of striatal neurons to synaptic input. *J Neurophysiol*. 2014;113(3):688–700.
58. Hu H, Gan J, Jonas P. Interneurons fast-spiking, parvalbumin + GABAergic interneurons: from cellular design to microcircuit function. *Science*. 2014;345(6196):1255263.
59. Siegle JH, Pritchett DL, Moore CI. Gamma-range synchronization of fast-spiking interneurons can enhance detection of tactile stimuli. *Nat Neurosci*. 2014;17(10):1371–9.
60. Brown P. Cortical drives to human muscle: the Piper and related rhythms. *Prog Neurobiol*. 2000;60(1):97–108.
61. McNally JM, McCarley RW. Gamma band oscillations: a key to understanding schizophrenia symptoms and neural circuit abnormalities. *Curr Opin Psychiatry*. 2016;29(3):202–10.
62. Tecuapetla F, Matias S, Dugue GP, Mainen ZF, Costa RM. Balanced activity in basal ganglia projection pathways is critical for contraversive movements. *Nat Commun*. 2014;5(4315):1–10.